A&A 566, A144 (2014)
DOI: 10.1051/0004-6361/201423733

Astronomy & Astrophysics

Ion-molecule reactions involving HCO^+ and N_2H^+: Isotopologue equilibria from new theoretical calculations and consequences for interstellar isotope fractionation

M. Mladenović[1] and E. Roueff[2]

[1] Université Paris-Est, Laboratoire Modélisation et Simulation Multi Echelle, MSME, UMR 8208 CNRS, 5 Bd Descartes, 77454 Marne la Vallée, France
e-mail: Mirjana.Mladenovic@u-pem.fr
[2] LERMA and UMR 8112 du CNRS, Observatoire de Paris, Section de Meudon, Place J. Janssen, 92195 Meudon, France
e-mail: evelyne.roueff@obspm.fr

Received 28 February 2014 / Accepted 14 April 2014

ABSTRACT

Aims. We revisit with new augmented accuracy the theoretical dynamics of basic isotope exchange reactions involved in the $^{12}C/^{13}C$, $^{16}O/^{18}O$, and $^{14}N/^{15}N$ balance because these reactions have already been studied experimentally in great detail.
Methods. Electronic structure methods were employed to explore potential energy surfaces, full-dimensional rovibrational calculations to compute rovibrational energy levels that are numerically exact, and chemical network models to estimate the abundance ratios under interstellar conditions.
Results. New exothermicities, derived for HCO^+ reacting with CO, provide rate coefficients markedly different from previous theoretical values in particular at low temperatures, resulting in new abundance ratios relevant for carbon chemistry networks. In concrete terms, we obtain a reduction in the abundance of $H^{12}C^{18}O^+$ and an increase in the abundance of $H^{13}C^{16}O^+$ and $D^{13}C^{16}O^+$. In all studied cases, the reaction of the ion with a neutral polarizable molecule proceeds through the intermediate proton-bound complex found to be very stable. For the complexes $OCH^+ \cdots CO$, $OCH^+ \cdots OC$, $COHOC^+$, $N_2 \cdots HCO^+$, $N_2H^+ \cdots OC$, and $N_2HN_2^+$, we also calculated vibrational frequencies and dissociation energies.
Conclusions. The linear proton-bound complexes possess sizeable dipole moments, which may facilitate their detection.

Key words. ISM: abundances – ISM: general – ISM: molecules

1. Introduction

Isotopic fractionation reactions have already been invoked by Watson (1976) and Dalgarno & Black (1976) to explain the enrichment of heavy isotopes of molecules in dark cold interstellar cloud environments. The exothermicity involved in the isotopic exchange reaction directly depends on the difference of the zero-point energies between the two isotopes, if one assumes that the reaction proceeds in the ground-rovibrational states of both the reactant and product molecule. This assumption has been questioned for the reaction $H_3^+ + HD \rightleftharpoons H_2D^+ + H_2$, where some rotational excitation in H_2 may reduce the efficiency of the reverse reaction (Pagani et al. 1992; Hugo et al. 2009).

In this paper we revisit some fractionation reactions involved in the $^{12}C/^{13}C$, $^{16}O/^{18}O$, and $^{14}N/^{15}N$ balance by reinvestigating the potential energy surfaces (PESs) involved in the isotopic exchange reactions. Within the Born-Oppenheimer approximation, a single nuclear-mass-independent PES is considered for all isotopic variants of molecules under consideration. The nuclear motions are introduced subsequently and isotopologues, molecules of different isotopic compositions and thus different masses, possess different rotational constants, different vibrational frequencies, and different ground-state (zero-point) vibrational energies, in other words, different thermodynamic properties (Urey 1947). Differences in zero-point energies can become important under cool interstellar cloud conditions where molecules rather undergo isotopic exchange (fractionation) than react chemically. This thermodynamic effect may result in isotopologue abundance ratios (significantly) deviating from the elemental isotopic ratios. Knowledge of the abundance ratios may in return provide valuable information on molecular processes at low collision energies.

As far as astrophysical models are concerned, ^{13}C and ^{18}O isotopic fractionation studies involving CO and HCO^+ (Le Bourlot et al. 1993; Liszt 2007; Röllig & Ossenkopf 2013; Maret et al. 2013) are based on the pionneering paper by Langer et al. (1984), who referred to the experimental studies by Smith & Adams (1980) and used theoretical spectroscopic parameters for the isotopic variants of HCO^+ reported by Henning et al. (1977). Lohr (1998) derived the harmonic frequencies and equilibrium rotational constants for CO, HCO^+, and HOC^+ at the configuration interaction (including single and double excitations) level of theory (CISD/6-31G**) and tabulated reduced partition function ratios and isotope exchange equilibrium constants for various isotope exchange reactions between CO and HCO^+. Surprisingly, this paper has not received much attention in the astrophysical literature, and its conclusions have never been applied.

The studies of Langer et al. (1984) and Lohr (1998) led to qualitatively different conclusions regarding the following

fractionation reaction:

$$^{13}C^{16}O + H^{12}C^{18}O^+ \rightarrow H^{13}C^{16}O^+ + {}^{12}C^{18}O + \Delta E, \quad (1)$$

which was found to be endothermic with $\Delta E/k_B = -5$ K by Langer et al. (1984) and exothermic with $\Delta E/k_B = 12.5$ K by Lohr (1998), where k_B is the Boltzmann constant. To clear up this discrepancy, we carried out numerically exact calculations for the vibrational ground state of HCO^+ using a PES previously developed by Mladenović & Schmatz (1998). Our calculations gave $\Delta E/k_B = 11.3$ K for reaction (1), in good agreement with the harmonic value of Lohr (1998). In addition, we noticed that the $\Delta E/k_B$ values of Henning et al. (1977) for the reactions

$$^{13}C^{16}O + H^{12}C^{16}O^+ \rightleftharpoons H^{13}C^{16}O^+ + {}^{12}C^{16}O \quad (2)$$

and

$$^{12}C^{18}O + H^{12}C^{16}O^+ \rightleftharpoons H^{12}C^{18}O^+ + {}^{12}C^{16}O \quad (3)$$

were quoted as 17 ± 1 K and 7 ± 1 K by Smith & Adams (1980) and as 9 and 14 K by Langer et al. (1984). Reconsidering the original values of Henning et al. (1977), we found that Langer et al. (1984) permuted the zero-point energies for $H^{13}C^{16}O^+$ and $H^{12}C^{18}O^+$ in Table 2 of their paper. From the original spectroscopic parameters of Henning et al. (1977), we derive $\Delta E/k_B = 10.2$ K for reaction (1), in good agreement with our result and the result of Lohr (1998).

The permutation of the zero-point vibrational energies of $H^{13}C^{16}O^+$ and $H^{12}C^{18}O^+$ affects the exothermicities and rate coefficients summarized in Tables 1 and 3 of the paper by Langer et al. (1984). These data are actually incorrect for all isotope fractionation reactions CO+HCO^+, except for

$$^{13}C^{18}O + H^{12}C^{16}O^+ \rightleftharpoons H^{13}C^{18}O^+ + {}^{12}C^{16}O. \quad (4)$$

The rate coefficients reported by Langer et al. (1984) are still widely used when including isotopes such as ^{13}C and ^{18}O into chemical (molecular) networks (Maret et al. 2013; Röllig & Ossenkopf 2013). With these points in mind, our goal is to provide reliable theoretical estimates for the zero-point vibrational energies first of H/DCO^+ and to derive proper rate coefficients for the related fractionation reactions. Our improved results for the exothermicities and rate coefficients are summarized in Tables 2 and 5.

Henning et al. (1977) also reported spectroscopic parameters for various isotopic variants of N_2H^+. This was our initial motivation to expand the present study to ion-molecule reactions between N_2H^+ and N_2. ^{15}N fractionation in dense interstellar clouds has been first considered by Terzieva & Herbst (2000), who referred to the experimental information of the selected ion flow-tube (SIFT) studies at low temperatures of Adams & Smith (1981).

The reactions discussed in this paper, CO+HCO^+ and $N_2 + HN_2^+$, are the most obvious candidates for isotopic fractionation. In addition, they have been studied in the laborataory, which allows a detailed discussion. A similar reaction has been invoked for CN (Milam et al. 2009), but no experimental and/or theoretical information is available there.

In the Langevin model, the long-range contribution to the intermolecular potential is described by the isotropic interaction between the charge of the ion and the induced dipole of the neutral. Theoretical approaches based on this standard assumption may qualitatively explain the behaviour of the association rates. However, they generally provide rate coefficients that are higher than experimental results (Langer et al. 1984). The rate coefficients for ion-molecule reactions are quite constant at higher temperatures but increase rapidly at lower temperatures. The latter feature is an indication of barrierless PESs. The electrostatic forces are always attractive and can be experienced over large distances even at extremely low temperatures relevant for dark cloud enviroments. Short-range forces appear in closer encounters of interacting particles and may (prominently) influence the overall reaction rate. To explore the short-range effects we also undertake a study of linear proton-bound ionic complexes arising in the reactions involving HCO^+, HOC^+, and N_2H^+ with CO and N_2, which are common interstellar species.

Our theoretical approach is described in Sect. 2. The specific aspects of the fractionation reactions of HCO^+ and HOC^+ with CO are reanalysed in Sect. 3.1 and the fractionation reactions $N_2H^+ + N_2$ in Sect. 3.2. We discuss the equilibrium constants and rate coefficients of CO+HCO^+/HOC^+ in Sect. 4.1, providing the astrochemical implications of the new exothermicities in Sect. 4.2. The isotope fractionation reactions $N_2H^+ + N_2$ are considered including the nuclear spin angular momentum selection rules in Sect. 4.3. The linear proton-bound cluster ions are analysed in Sect. 4.4. Our concluding remarks are given in Sect. 5.

2. Calculations

The global three-dimensional PES developed by Mladenović & Schmatz (1998) for the isomerizing system HCO^+/HOC^+ and by Schmatz & Mladenović (1997) for the isoelectronic species N_2H^+ were used in the rovibrational calculations. These two PESs still provide the most comprehensive theoretical descriptions of the spectroscopic properties for HCO^+, HOC^+, and N_2H^+ and are valid up to the first dissociation limit. Potential energy representations recently developed by Špirko et al. (2008) and by Huang et al. (2010) reproduce the experimental fundamental transitions within 11[6] and 4[3] cm^{-1} for N_2H^+[N_2D^+], respectively, whereas the PES of Schmatz & Mladenović (1997) predicts the fundamental transitions for both N_2H^+ and N_2D^+ within 2 cm^{-1}.

The rovibrational energy levels of HCO^+/HOC^+ and N_2H^+ are calculated by a numerically exact quantum mechanical method, involving no dynamical approximation and applicable to any potential energy representation. The computational strategy is based on the discrete variable representation of the angular coordinate in combination with a sequential diagonalization/truncation procedure (Mladenović & Bačić 1990; Mladenović & Schmatz 1998). For both molecular systems, the rovibrational states are calculated for the total angular momentum $J = 0-15$. These rovibrational energies are used to evaluate theoretical partition functions and to model rate coefficients for proton transfer reactions involving HCO^+ and N_2H^+.

To gain a first insight into dynamical features of ion-molecule reactions, additional electronic structure calculations were carried out for linear proton-bound cluster ions of HCO^+, HOC^+, and N_2H^+ with CO and N_2. The PESs were scanned by means of the coupled cluster method with single and double excitations including perturbative corrections for triple excitations [CCSD(T)] in combination with the augmented correlation consistent triple ζ basis set (aug-cc-pVTZ). Only valence electrons were correlated. The ab initio calculations were carried out with the MOLPRO (Werner et al. 2012) and CFOUR (Stanton et al. 2012) quantum chemistry program packages.

3. Results

The PES of Mladenović & Schmatz (1998) provides a common potential energy representation for the formyl cation, HCO^+, and

Table 1. Zero-point vibrational energies (in cm^{-1}) of isotopologues of CO, HCO^+, and HOC^+.

Species	This work	L98[a]	MTL93[b]	LGFA84[c]	HKD77[d]	HH79[e]
$^{12}C^{16}O$	1079.11	1131.9		1084.8		1081.6
$^{13}C^{16}O$	1055.12	1106.8		1060.6		1057.5
$^{12}C^{18}O$	1053.11	1104.8		1059.0		1055.5
$^{13}C^{18}O$	1028.52	1078.7		1034.0		1030.7
$H^{12}C^{16}O^+$	3524.60	3713.6	3512.3	3487.6	3487.6	
$H^{13}C^{16}O^+$	3488.24	3674.6	3475.89[f]	3457.0	3452.0	
$H^{12}C^{18}O^+$	3494.15	3681.3		3452.1	3457.1	
$H^{13}C^{18}O^+$	3457.16	3641.6		3421.5	3421.1	
$D^{12}C^{16}O^+$	2944.22	3096.4			2918.9	
$D^{13}C^{16}O^+$	2905.16	3055.0			2880.4	
$D^{12}C^{18}O^+$	2912.86	3063.4			2887.7	
$D^{13}C^{18}O^+$	2873.18	3021.7			2848.5	
$H^{16}O^{12}C^+$	2871.08	2874.3	2907.4		2934.4	
$H^{16}O^{13}C^+$	2848.66	2851.0			2911.3	
$H^{18}O^{12}C^+$	2841.37	2844.4			2905.0	
$H^{18}O^{13}C^+$	2818.42	2820.5			2881.5	
$D^{16}O^{12}C^+$	2357.61	2365.6			2411.6	
$D^{16}O^{13}C^+$	2334.87	2341.9			2389.0	
$D^{18}O^{12}C^+$	2326.06	2335.0			2381.1	
$D^{18}O^{13}C^+$	2302.82	2311.0			2357.8	

References. [(a)] Lohr (1998). [(b)] Martin et al. (1993). [(c)] Langer et al. (1984). [(d)] Computed from the original data of Henning et al. (1977). [(e)] Huber & Herzberg (1979) [(f)] T. J. Lee, priv. comm.

the isoformyl cation, HOC^+, where the local HOC^+ minimum is 13 878 cm^{-1} (166 kJ mol^{-1}) above the global HCO^+ minimum. Inclusion of the zero-point energy reduces this separation by 640–650 cm^{-1} for the hydrogen-containing isotopologues and by 570–580 cm^{-1} for the deuterium variants. The angular motion is described by a double-minimum anharmonic potential with a non-linear saddle point at 26 838 cm^{-1} (321 kJ mol^{-1}) above the HCO^+ minimum, such that low-lying states of HCO^+ and HOC^+ are well separated.

The PES of Schmatz & Mladenović (1997) for N_2H^+ (dyazenilium) has two equivalent colinear minima as a consequence of the S_2 permutation symmetry, separated by an isomerization barrier 17 137 cm^{-1} (205 kJ mol^{-1}) above the energy of the linear geometries. Low-lying states of N_2H^+ are, thus, localized in one of the two wells. The double-well symmetry and nuclear spin symmetries are lifted for mixed nitrogen isotope forms.

3.1. Reaction of CO with HCO^+ and HOC^+

The ground-state vibrational energies calculated in this work for isotopic variants of HCO^+ and HOC^+ are collected in Table 1. There we additionally show the harmonic zero-point energy estimates of Lohr (1998) and the anharmonic values of Martin et al. (1993) available only for three isotopologues, as well as the values obtained by Langer et al. (1984) and in the present work from the spectroscopic [CI(corr)] parameters of Henning et al. (1977). Our values for CO are computed at the theoretical level used to construct the PES for HCO^+/HOC^+ [CCSD(T)/cc-pVQZ].

The isotopologues in Table 1 are arranged in order of increasing total molecular mass. For CO and H/DOC^+, the zero-point energies decrease as the total molecular mass increases, which is not the case for H/DCO^+. Inspection of the table shows that the substitution of the central atom by its heavier isotope ($^{12}C\rightarrow^{13}C$ in H/DCO^+ and $^{16}O\rightarrow^{18}O$ in H/DOC^+) results in a more pronounced decrease of the zero-point energy than the isotopic substitution of the terminal atom ($^{16}O\rightarrow^{18}O$ in H/DCO^+ and $^{12}C\rightarrow^{13}C$ in H/DOC^+). This feature shared by H/DCO^+ and H/DOC^+ in Table 1 is easy to rationalize since a central atom substitution affects all three vibrational frequencies.

The zero-point energy differences for the proton transfer reactions $CO+HCO^+/HOC^+$ are listed in Table 2. The reactions involving the formyl cation are labelled with F and the reactions involving the isoformyl cation with I. The deuterium variant of reaction F1 is denoted by F1(D) and similar for all other reactions. The reactions F1, F2, F3, F4, F5, and F6 are numbered as 1004, 3408, 3407, 3457, 3406, and 3458 by Langer et al. (1984).

In Table 2, our results, the values rederived from the spectroscopic parameters of Henning et al. (column HKD77), and the harmonic values of Lohr (column L98) all agree within less than 5 K. These three data sets predict the same direction for all listed reactions, whereas Langer et al. (column LGFA84) reported reaction F6 as endothermic. The replacement of our theoretical values for CO by the experimental values taken from Huber & Herzberg (1979) affects the zero-point energy differences by at most 0.4 K.

The general trend seen in Table 2 is that ^{13}C is preferentially placed in H/DCO^+ and ^{18}O in H/DOC^+. This is in accordance with Table 1, showing a stronger decrease of the zero-point energy upon isotopic substitution of the central atom. The substitution of the two ^{16}O by ^{18}O or the two ^{12}C by ^{13}C has nearly no influence on the exothermicities, as seen by comparing ΔE for reactions F1, F1(D), I1, I1(D) with ΔE for reactions F2, F2(D), I2, I2(D) and silimar for reactions F3, F3(D), I3, I3(D) versus F4, F4(D), I4, I4(D). Slightly higher exothermicities appear for reactions involving deuterium. The exothermicities for the reactions with the isoformyl isomers are lower than for the reactions with the formyl forms.

Table 2. Zero-point energy differences (in K) between the reactants and products for the isotope fractionation reactions of H/DCO$^+$ and H/DOC$^+$ with CO.

		Theory				Exp
Label	Reaction	This work[a]	L98[b]	HKD77[c]	LGFA84[d]	SA80[e]
	$^{13}C^+ + {}^{12}C^{16}O \rightarrow {}^{12}C^+ + {}^{13}C^{16}O$	34.5 [34.7]	36.0		35	40 ± 6
	$^{13}C^+ + {}^{12}C^{18}O \rightarrow {}^{12}C^+ + {}^{13}C^{18}O$	35.4 [35.6]	37.5		36	
F1	$H^{12}C^{16}O^+ + {}^{13}C^{16}O \rightarrow H^{13}C^{16}O^+ + {}^{12}C^{16}O$	17.8 [17.6]	20.0	16.5	9	12 ± 5
F2	$H^{12}C^{18}O^+ + {}^{13}C^{18}O \rightarrow H^{13}C^{18}O^+ + {}^{12}C^{18}O$	17.8 [17.6]	19.5	16.4	8	
F3	$H^{12}C^{16}O^+ + {}^{12}C^{18}O \rightarrow H^{12}C^{18}O^+ + {}^{12}C^{16}O$	6.4 [6.2]	7.5	6.2	14	15 ± 5
F4	$H^{13}C^{16}O^+ + {}^{13}C^{18}O \rightarrow H^{13}C^{18}O^+ + {}^{13}C^{16}O$	6.4 [6.2]	7.0	6.1	13	
F5	$H^{12}C^{16}O^+ + {}^{13}C^{18}O \rightarrow H^{13}C^{18}O^+ + {}^{12}C^{16}O$	24.2 [23.9]	27.0	22.6	22	
F6	$H^{12}C^{18}O^+ + {}^{13}C^{16}O \rightarrow H^{13}C^{16}O^+ + {}^{12}C^{18}O$	11.4 [11.4]	12.5	10.3	–5	≤5
F1(D)	$D^{12}C^{16}O^+ + {}^{13}C^{16}O \rightarrow D^{13}C^{16}O^+ + {}^{12}C^{16}O$	21.7 [21.5]	23.5	20.7		
F2(D)	$D^{12}C^{18}O^+ + {}^{13}C^{18}O \rightarrow D^{13}C^{18}O^+ + {}^{12}C^{18}O$	21.7 [21.5]	22.5	20.9		
F3(D)	$D^{12}C^{16}O^+ + {}^{12}C^{18}O \rightarrow D^{12}C^{18}O^+ + {}^{12}C^{16}O$	7.7 [7.5]	8.5	7.3		
F4(D)	$D^{13}C^{16}O^+ + {}^{13}C^{18}O \rightarrow D^{13}C^{18}O^+ + {}^{13}C^{16}O$	7.7 [7.5]	7.5	7.5		
F5(D)	$D^{12}C^{16}O^+ + {}^{13}C^{18}O \rightarrow D^{13}C^{18}O^+ + {}^{12}C^{16}O$	29.4 [29.0]	31.0	28.2		
F6(D)	$D^{12}C^{18}O^+ + {}^{13}C^{16}O \rightarrow D^{13}C^{16}O^+ + {}^{12}C^{18}O$	14.0 [14.0]	15.0	13.4		
I1	$H^{16}O^{12}C^+ + {}^{13}C^{16}O \rightarrow H^{16}O^{13}C^+ + {}^{12}C^{16}O$	–2.3 [–2.4]	–2.5	–1.5		
I2	$H^{18}O^{12}C^+ + {}^{13}C^{18}O \rightarrow H^{18}O^{13}C^+ + {}^{12}C^{18}O$	–2.4 [-2.6]	–3.0	–1.7		
I3	$H^{16}O^{12}C^+ + {}^{12}C^{18}O \rightarrow H^{18}O^{12}C^+ + {}^{12}C^{16}O$	5.3 [5.2]	4.0	4.7		
I4	$H^{16}O^{13}C^+ + {}^{13}C^{18}O \rightarrow H^{18}O^{13}C^+ + {}^{13}C^{16}O$	5.2 [5.0]	3.5	4.5		
I5	$H^{16}O^{12}C^+ + {}^{13}C^{18}O \rightarrow H^{18}O^{13}C^+ + {}^{12}C^{16}O$	3.0 [2.6]	1.0	3.0		
I6	$H^{18}O^{12}C^+ + {}^{13}C^{16}O \rightarrow H^{16}O^{13}C^+ + {}^{12}C^{18}O$	–7.6 [–7.6]	–6.5	–6.2		
I1(D)	$D^{16}O^{12}C^+ + {}^{13}C^{16}O \rightarrow D^{16}O^{13}C^+ + {}^{12}C^{16}O$	–1.8 [–2.0]	–2.0	–2.1		
I2(D)	$D^{18}O^{12}C^+ + {}^{13}C^{18}O \rightarrow D^{18}O^{13}C^+ + {}^{12}C^{18}O$	–1.9 [–2.1]	–3.0	–2.0		
I3(D)	$D^{16}O^{12}C^+ + {}^{12}C^{18}O \rightarrow D^{18}O^{12}C^+ + {}^{12}C^{16}O$	8.0 [7.8]	5.0	6.2		
I4(D)	$D^{16}O^{13}C^+ + {}^{13}C^{18}O \rightarrow D^{18}O^{13}C^+ + {}^{13}C^{16}O$	7.8 [7.6]	4.0	6.3		
I5(D)	$D^{16}O^{12}C^+ + {}^{13}C^{18}O \rightarrow D^{18}O^{13}C^+ + {}^{12}C^{16}O$	6.0 [5.7]	2.0	4.2		
I6(D)	$D^{18}O^{12}C^+ + {}^{13}C^{16}O \rightarrow D^{16}O^{13}C^+ + {}^{12}C^{18}O$	–9.8 [–9.8]	–7.0	–8.4		

Notes. [(a)] Zero-point energy differences obtained using experimental CO zero-point values from Huber & Herzberg (1979) are given in brackets. [(b)] Lohr (1998) [(c)] computed from the original data of Henning et al. (1977) [(d)] Langer et al. (1984) [(e)] Smith & Adams (1980) .

From the measured forward reaction k_f and backward reaction k_r rate coefficients, Smith & Adams (1980) calculated the experimental zero-point energy differences using

$$\frac{k_f}{k_r} = K_e = e^{\Delta E/k_B T}, \quad (5)$$

where K_e is the equilibrium constant. The total estimated error on k_f and k_r is reported to be ±25% at 80 K. Table 2 indicates that the new/improved theoretical values, and the experimental finding for reaction F1 agree within the experimental uncertainty. For reactions F3 and F6, we see that the theoretical results consistently predict a higher ΔE value for $H^{12}C^{18}O^+$ reacting with $^{13}C^{16}O$ (reaction F6) than for $H^{12}C^{16}O^+$ reacting with $^{12}C^{18}O$ (reaction F3), whereas the opposite was derived experimentally. Note that Smith & Adams (1980) reported for $^{13}C^{16}O$ reacting with $H^{12}C^{18}O^+$ in addition to reaction F6 also a yield of 10% for the rearrangement channel

$$^{13}C^{16}O + H^{12}C^{18}O^+ \rightarrow H^{13}C^{18}O^+ + {}^{12}C^{16}O. \quad (6)$$

The latter transformation is not of a simple proton-transfer type (but bond-rearrangement type) and must involve a more complicated chemical mechanism probably including an activation energy barrier.

3.2. Reaction of N_2 with N_2H^+

The zero-point vibrational energies calculated for N_2H^+ are summarized in Table 3. In addition to the results obtained for the PES of Schmatz & Mladenović (1997), Table 3 also provides the values we derived from the spectroscopic parameters of Huang et al. (2010, column HVL10) and of Henning et al. (1977, column HKD77). The values for N_2 are taken from Huber & Herzberg (1979). The zero-point energy differences are given in Table 4. As seen there, our results agree with the values obtained

Table 3. Zero-point vibrational energies (in cm^{-1}) of isotopologues of N_2 and N_2H^+.

Species	This work	HVL10[a]	HKD77[b]	HH79[c]
$^{14}N^{14}N$				1175.7
$^{14}N^{15}N$				1156.0
$^{15}N^{15}N$				1136.0
$H^{14}N^{14}N^+$	3507.79	3508.6	3468.6	
$H^{15}N^{14}N^+$	3480.90	3481.8	3442.6	
$H^{14}N^{15}N^+$	3486.67	3487.5	3447.6	
$H^{15}N^{15}N^+$	3459.44	3460.4	3420.9	
$D^{14}N^{14}N^+$	2921.18	2917.1	2892.5	
$D^{15}N^{14}N^+$	2892.33	2888.3	2864.7	
$D^{14}N^{15}N^+$	2899.54	2895.6	2871.2	
$D^{15}N^{15}N^+$	2870.36	2866.6	2843.1	

Notes. [(a)] Computed from the original data of Huang et al. (2010); [(b)] computed from the original data of Henning et al. (1977); [(c)] Huber & Herzberg (1979) .

Table 4. Zero-point energy differences (in K) between the reactants and products for the isotope fractionation reactions of N_2H^+ with N_2.

		Theory				Exp
Label	Reaction	This work	HVL10[a]	TH00[b]	HKD77[c]	AS81[d]
D1	$^{14}N_2H^+ + {}^{15}N_2 \rightarrow {}^{15}N_2H^+ + {}^{14}N_2$	12.4	12.0		11.3	13 ± 3
D2	$^{14}N_2H^+ + {}^{15}N^{14}N \rightarrow {}^{14}N^{15}NH^+ + {}^{14}N_2$	10.3	10.1	10.7	9.0	9 ± 3
D3	$^{14}N_2H^+ + {}^{15}N^{14}N \rightarrow {}^{15}N^{14}NH^+ + {}^{14}N_2$	2.0	1.9	2.25	1.9	
D4	$^{14}N^{15}NH^+ + {}^{15}N_2 \rightarrow {}^{15}N_2H^+ + {}^{15}N^{14}N$	2.0	1.9		2.3	9 ± 3
D5	$^{15}N^{14}NH^+ + {}^{15}N_2 \rightarrow {}^{15}N_2H^+ + {}^{15}N^{14}N$	10.3	10.1		9.4	
D6	$^{15}N^{14}NH^+ + {}^{15}N^{14}N \rightarrow {}^{14}N^{15}NH^+ + {}^{14}N^{15}N$	8.3	8.2		7.1	
D1(D)	$^{14}N_2D^+ + {}^{15}N_2 \rightarrow {}^{15}N_2D^+ + {}^{14}N_2$	15.9	15.6		14.0	
D2(D)	$^{14}N_2D^+ + {}^{15}N^{14}N \rightarrow {}^{14}N^{15}ND^+ + {}^{14}N_2$	13.2	13.1		11.7	
D3(D)	$^{14}N_2D^+ + {}^{15}N^{14}N \rightarrow {}^{15}N^{14}ND^+ + {}^{14}N_2$	2.8	2.6		2.4	
D4(D)	$^{14}N^{15}ND^+ + {}^{15}N_2 \rightarrow {}^{15}N_2D^+ + {}^{15}N^{14}N$	2.8	2.5		2.3	
D5(D)	$^{15}N^{14}ND^+ + {}^{15}N_2 \rightarrow {}^{15}N_2D^+ + {}^{15}N^{14}N$	13.1	12.9		11.6	
D6(D)	$^{15}N^{14}ND^+ + {}^{15}N^{14}N \rightarrow {}^{14}N^{15}ND^+ + {}^{14}N^{15}N$	10.4	10.4		9.2	

Notes. [(a)] Computed from the original data of Huang et al. (2010); [(b)] Terzieva & Herbst (2000); [(c)] computed from the original data of Henning et al. (1977); [(d)] Adams & Smith (1981).

from the spectroscopic parameters of Huang et al. (2010) within 0.4 K. The reactions involving diazenylium (or dinitrogen monohydride cation) are labelled with D in Table 4.

The $^{14}N/^{15}N$ substitution at the central-atom position lowers the zero-point energy more than the terminal-atom substitution (Table 3), such that ^{15}N preferentially assumes the central position in N-N-H^+ in all reactions of N_2H^+ with N_2 in Table 4. The exothermicities are found to be slightly higher for the reactions involving deuterium.

In Table 4, the experimental (SIFT) results of Adams & Smith (1981) are listed as given in their paper. Note, however, that the elementary isotope fractionation reactions D2 and D3

$$^{14}N_2H^+ + {}^{15}N^{14}N \underset{k_{-2}}{\overset{k_2}{\rightleftharpoons}} {}^{14}N^{15}NH^+ + {}^{14}N_2, \tag{7}$$

$$^{14}N_2H^+ + {}^{15}N^{14}N \underset{k_{-3}}{\overset{k_3}{\rightleftharpoons}} {}^{15}N^{14}NH^+ + {}^{14}N_2, \tag{8}$$

involve common reactants, whereas reactions D4 and D5

$$^{14}N^{15}NH^+ + {}^{15}N_2 \underset{k_{-4}}{\overset{k_4}{\rightleftharpoons}} {}^{15}N_2H^+ + {}^{15}N^{14}N, \tag{9}$$

$$^{15}N^{14}NH^+ + {}^{15}N_2 \underset{k_{-5}}{\overset{k_5}{\rightleftharpoons}} {}^{15}N_2H^+ + {}^{15}N^{14}N, \tag{10}$$

have common products. The two reaction pairs are related by the $^{14}N \rightarrow {}^{15}N$ substitution. Using thermodynamic reasoning, it is easy to verify that the following relationship

$$\frac{K_e^{(2)}}{K_e^{(3)}} = \frac{K_e^{(5)}}{K_e^{(4)}} = K_e^{(6)} \tag{11}$$

is strictly fulfilled for $K_e^{(i)} = k_i/k_{-i}$, where $K_e^{(6)}$ corresponds to reaction D6,

$$^{15}N^{14}NH^+ + {}^{15}N^{14}N \underset{k_{-6}}{\overset{k_6}{\rightleftharpoons}} {}^{14}N^{15}NH^+ + {}^{14}N^{15}N. \tag{12}$$

Note that the factor $1/K_e^{(6)}$ also provides the thermal population of $^{15}N^{14}NH^+$ relative to $^{14}N^{15}NH^+$.

4. Discussion

The equilibrium constant K_e for the proton transfer reaction

$$A + HB \underset{k_r}{\overset{k_f}{\rightleftharpoons}} HA + B \tag{13}$$

under thermal equilibrium conditions is given by

$$K_e = \frac{k_f}{k_r} = \frac{Q(HA)}{Q(HB)}\frac{Q(B)}{Q(A)}, \tag{14}$$

where $Q(X)$ is the full partition function for the species X. Making the translation contribution explicit, we obtain

$$K_e = f_m^{3/2}\,\frac{Q_{int}(HA)}{Q_{int}(HB)}\frac{Q_{int}(B)}{Q_{int}(A)}\,e^{\Delta E/k_B T}, \tag{15}$$

where the mass factor f_m is given by

$$f_m = \frac{m(HA)\,m(B)}{m(HB)\,m(A)} \tag{16}$$

for $m(X)$ denoting the mass of the species X, whereas ΔE stands for the zero-point energy difference between the reactants and the products,

$$\Delta E = E_0^{HB} + E_0^{A} - E_0^{HA} - E_0^{B}. \tag{17}$$

The zero-point energies E_0 are measured on an absolute energy scale. For isotope fractionation reactions, the internal partition function, Q_{int}, includes only the rovibrational degrees of freedom (no electronic contribution) and is given by the standard expression

$$Q_{int} = g \sum_J \sum_i (2J+1)\, e^{-\varepsilon_i^J/k_B T}, \tag{18}$$

where $\varepsilon_i^J = E_i^J - E_0^0$ for a total angular momentum J is the rovibrational energy measured relative to the corresponding zero-point energy ($J = 0$). The factor $(2J + 1)$ accounts for the degeneracy relative to the space-fixed reference frame and g for the nuclear spin (hyperfine) degeneracy,

$$g = \Pi_\alpha (2I_{N,\alpha} + 1), \tag{19}$$

in which α labels the constituent nuclei having the nuclear spin $I_{N,\alpha}$. For the nuclei considered in the present work, we have $I_N(H) = 1/2$, $I_N(D) = 1$, $I_N(^{12}C) = 0$, $I_N(^{13}C) = 1/2$, $I_N(^{16}O) = 0$, $I_N(^{18}O) = 0$, $I_N(^{14}N) = 1$, and $I_N(^{15}N) = 1/2$.

Introducing the ratio

$$R_Y^X = \frac{Q_{int}(X)}{Q_{int}(Y)}, \quad (20)$$

the equilibrium constant is compactly written as

$$K_e = \frac{k_f}{k_r} = F_q \, e^{\Delta E/k_B T}, \quad (21)$$

where the partition function factor F_q is

$$F_q = f_m^{3/2} R_{HB}^{HA} R_A^B. \quad (22)$$

For reactions proceeding in the ground-rovibrational states of the reactants and the products, the partition function ratios R_{HB}^{HA} and R_A^B are both equal to 1. Even then the corresponding partition function factor F_q of Eq. (22) is, strictly speaking, different from 1 because of the mass term f_m defined by Eq. (16). For the reactions F1–F6 in Table 2, for instance, the $f_m^{3/2}$ values are 0.998, 0.998, 0.997, 0.997, 0.995, and 1.002, respectively, which are different from 1 at most by 0.5%. The $f_m^{3/2}$ values are computed from Eq. (16) using the following atomic masses $m(H) = 1.007825035$, $m(D) = 2.014101779$, $m(^{12}C) = 12$, $m(^{13}C) = 13.003354826$, $m(^{16}O) = 15.99491463$, and $m(^{18}O) = 17.9991603$ u, as given by Mills et al. (1993).

The terms of Q_{int} in Eq. (18) decrease rapidly with energy and J. In the low-temperature limit relevant for dark cloud conditions, the discrete rotational structure of the ground-vibrational state provides the main contribution to Q_{int}. That said, the rotational energy cannot be treated as continuous and one must explicitly sum the terms to obtain Q_{int}. With increasing temperature, the rotational population in the ground-vibrational state increases and other vibrational states may also become accessible, leading to partition function factors F_q, which may show (weak) temperature dependences.

For a given PES, numerically exact full-dimensional strategies insure the determination of accurate level energies and therefore accurate partition functions and equilibrium constants. To predict/estimate rate coefficients, we may use kinetic models, such as e.g. the Langevin collision rate model for ion-molecule reactions. Uncertainties in the rate coefficients are thus defined by uncertainties in the model parameters. In the case of the system CO+HCO$^+$, we employ the total rate coefficients from Table 3 of Langer et al. (1984) and the uncertainties of these quantities also provide the uncertainties of the rate coefficients derived in the present work.

4.1. Reaction of CO with HCO$^+$

The equilibrium constants for HCO$^+$ reacting with CO are given in Table 5. Our K_e values are obtained in accordance with Eq. (21) by direct evaluation of the internal partition functions Q_{int} from the computed rovibrational energies. The forward reaction k_f and backward reaction k_r rate coefficients are calculated using our ΔE values and the total temperature-dependent rate coefficients k_T given by Langer et al. (1984), where

$$k_T = k_f + k_r, \quad (23)$$

such that

$$k_f = k_T K_e/(K_e + 1), \quad (24)$$

$$k_r = k_T/(K_e + 1). \quad (25)$$

The results for the deuterium variants are also listed in Table 5. Their rate coefficients k_f and k_r are calculated assuming the same total rate coefficients k_T as for the H-containing forms (due to nearly equal reduced masses). For the purpose of comparison, note that the Langevin rate for CO+HCO$^+$ is $k_L = 8.67 \times 10^{-10}$ cm^3 s^{-1}.

The partition function factors F_q deviate from 1 by approximately 2% in Table 5. They also exhibit marginal temperature dependences. This reflects the influence of rotational and vibrational excitations in the reactants and the products. Only the rotationally excited ground-vibrational states contribute to Q_{int} at temperatures $T < 200$ K. The contribution of the bending ν_2 level is 0.5% at 200 K and 3.6–3.8% at 300 K, whereas the contributions from $2\nu_2$ are 0.1% at 300 K. To appreciate the effect of F_q, we employed the rate coefficients measured at 80 K by Smith & Adams (1980) to determine the ΔE value for reactions F1, F3, and F6 by means of Eq. (21). Using the F_q values from Table 5, we obtain $\Delta E/k_B$ of 13.8, 15.1, and 4.8 K, respectively. For $F_q = 1$, we find 12.3, 14.6, and 3.8 K, which are lower by 1.5 K (12%), 0.5 K (3%), and 1 K (26%) than the former $F_q \neq 1$ results.

The equilibrium constants K_e reported by Langer et al. (1984) deviate from the present results and those of Lohr (1998) very prominently at low temperatures in Table 5. At 10 K, we see deviations of 43% and 217% with respect to our values for reactions F1 and F3, respectively, and the related rate coefficients k_f, k_r are accordingly different. An even larger discrepancy is seen for reaction F6 of Eq. (1), which was previously predicted to be endothermic. In accordance with this, the values of k_f and k_r derived by Langer et al. (1984) are given in the reverse positions as (k_r, k_f) for reaction F6 in Table 5.

The deuterium variants in Table 5 are associated with slightly lower F_q values and somewhat higher low-temperature K_e, resulting in somewhat faster foward reactions and slower backward reactions.

4.2. Astrochemical implications

We investigated the role of these new derived exothermicities under different density conditions relevant to cold dark interstellar clouds. We display in Table 6 steady-state results for isotopic ratios of CO, HCO$^+$ and DCO$^+$ for two chemical models performed at a temperature of 10 K with a cosmic ionization rate ζ of 1.3×10^{-17} s^{-1} per H_2 molecule with the old ΔE values by Langer et al. (Model A: LGFA84) and the present ΔE values listed in Table 2 (Model B). The ratios of the principal isotope to the minor isotope obtained for Model A, R_A, and for Model B, R_B, are compared using the relative difference δ,

$$\delta = 1 - R_B/R_A. \quad (26)$$

The chemical network contains 288 chemical species including ^{13}C and ^{18}O containing molecules as well as deuterated species and more than 5000 reactions. We assumed that the elemental ^{12}C/^{13}C and ^{16}O/^{18}O isotopic ratios are 60 and 500, so that any deviation relative to these values measures the amount of enrichment/depletion with respect to the elemental ratios. For the ^{13}C^{18}O-containing molecules the value of 30 000 is the reference. The zero-point energies of other isotopic substitutes do not pose any problem because the reactions involved in the interstellar chemical networks are significantly exothermic and the solutions of the chemical equations are independent of these quantities.

The isotopic fractionation reactions are introduced explicitly in the chemical network, whereas the other reactions involving

Table 5. Equilibrium constants K_e, partition function factors F_q, and rate coefficients k_f, k_r (in 10^{-10} cm^3 s^{-1}) for the reactions of H/DCO$^+$ with CO.

Reaction	T (K)	5	10	20	40	60	80	100	200	300
F1	F_q	0.9854	0.9832	0.9821	0.9816	0.9814	0.9813	0.9813	0.9815	0.9824
	K_e	34.64	5.83	2.39	1.53	1.32	1.23	1.17	1.07	1.04
	K_e(see *a*)		6.69					1.19	1.08	1.05
	K_e(see *b*)	6.0	2.5	1.6	1.3	1.2	1.1	1.1	1.0	1.0
	(k_f, k_r)	(9.33, 0.27)	(7.85, 1.35)	(6.35, 2.65)	(5.20, 3.40)	(4.67, 3.53)	(4.30, 3.50)	(4.05, 3.45)	(3.21, 2.99)	(2.65, 2.55)
	$(k_f, k_r)^b$	(8.2, 1.4)	(6.5, 2.7)	(5.5, 3.5)	(4.8, 3.8)	(4.4, 3.8)	(4.1, 3.7)	(3.9, 3.6)	(3.2, 3.0)	(2.6, 2.6)
	$(k_f, k_r)^c$						(4.2, 3.6)		(3.2, 3.0)	(2.6, 2.5)
F2	F_q	0.9853	0.9831	0.9821	0.9816	0.9814	0.9813	0.9813	0.9814	0.9822
	K_e	34.93	5.85	2.40	1.53	1.32	1.23	1.17	1.07	1.04
	K_e(see *a*)		6.65					1.19	1.08	1.05
	K_e(see *b*)	6.0	2.5	1.6	1.3	1.2	1.1	1.1	1.0	1.0
	(k_f, k_r)	(9.3, 0.27)	(7.86, 1.34)	(6.35, 2.65)	(5.21, 3.39)	(4.67, 3.53)	(4.30, 3.50)	(4.05, 3.45)	(3.21, 2.99)	(2.65, 2.55)
	$(k_f, k_r)^b$	(8.2, 1.4)	(6.5, 2.7)	(5.5, 3.5)	(4.8, 3.8)	(4.4, 3.8)	(4.1, 3.7)	(3.9, 3.6)	(3.2, 3.0)	(2.6, 2.6)
F3	F_q	0.9964	0.9951	0.9945	0.9942	0.9941	0.9941	0.9941	0.9941	0.9946
	K_e	3.59	1.89	1.37	1.17	1.11	1.08	1.06	1.03	1.02
	K_e(see *b*)	16.4	4.1	2.0	1.4	1.3	1.2	1.2	1.1	1.0
	(k_f, k_r)	(7.51, 2.09)	(6.01, 3.19)	(5.20, 3.80)	(4.63, 3.97)	(4.31, 3.89)	(4.04, 3.76)	(3.86, 3.64)	(3.14, 3.06)	(2.62, 2.58)
	$(k_f, k_r)^b$	(9.0, 0.6)	(7.4, 1.8)	(6.0, 3.0)	(5.0, 3.6)	(4.6, 3.6)	(4.2, 3.6)	(4.0, 3.5)	(3.2, 3.0)	(2.7, 2.5)
	$(k_f, k_r)^c$						(4.2, 3.5)		(3.2, 2.9)	(2.7, 2.6)
F4	F_q	0.9963	0.9951	0.9945	0.9942	0.9941	0.9941	0.9940	0.9941	0.9943
	K_e	3.61	1.90	1.37	1.17	1.11	1.08	1.06	1.03	1.02
	K_e(see *b*)	16.4	4.1	2.0	1.4	1.3	1.2	1.2	1.1	1.0
	(k_f, k_r)	(7.52, 2.08)	(6.02, 3.18)	(5.21, 3.79)	(4.63, 3.97)	(4.31, 3.89)	(4.05, 3.75)	(3.86, 3.64)	(3.14, 3.06)	(2.62, 2.58)
	$(k_f, k_r)^b$	(9.0, 0.6)	(7.4, 1.8)	(6.0, 3.0)	(5.0, 3.6)	(4.6, 3.6)	(4.2, 3.6)	(4.0, 3.5)	(3.2, 3.0)	(2.7, 2.5)
F5	F_q	0.9818	0.9783	0.9767	0.9759	0.9756	0.9755	0.9754	0.9756	0.9769
	K_e	125.26	11.05	3.28	1.79	1.46	1.32	1.24	1.10	1.06
	K_e(see *a*)		13.37					1.27	1.11	1.06
	K_e(see *b*)	81.5	9.0	3.0	1.7	1.4	1.3	1.2	1.1	1.1
	(k_f, k_r)	(9.52, 0.08)	(8.44, 0.76)	(6.90, 2.10)	(5.52, 3.08)	(4.87, 3.33)	(4.44, 3.36)	(4.16, 3.34)	(3.25, 2.95)	(2.67, 2.53)
	$(k_f, k_r)^b$	(9.5, 0.1)	(8.3, 0.9)	(6.8, 2.2)	(5.5, 3.1)	(4.8, 3.4)	(4.4, 3.4)	(4.2, 3.3)	(3.3, 2.9)	(2.7, 2.5)
F6	F_q	0.9890	0.9880	0.9875	0.9873	0.9872	0.9872	0.9872	0.9873	0.9878
	K_e	9.66	3.09	1.75	1.31	1.19	1.14	1.11	1.04	1.03
	K_e(see *a*)		3.33					1.11	1.05	1.03
	K_e(see *b*)	0.37	0.61	0.78	0.88	0.92	0.94	0.95	0.98	0.98
	(k_f, k_r)	(8.70, 0.90)	(6.95, 2.25)	(5.72, 3.28)	(4.88, 3.72)	(4.46, 3.74)	(4.15, 3.65)	(3.94, 3.56)	(3.17, 3.03)	(2.63, 2.57)
	$(k_r, k_f)^b$	(3.0, 6.6)	(3.7, 5.5)	(4.1, 4.9)	(4.1, 4.5)	(4.0, 4.2)	(3.8, 4.0)	(3.7, 3.8)	(3.1, 3.1)	(2.6, 2.6)
	$(k_f, k_r)^c$						(4.3, 4.1)		(3.1, 3.2)	(2.6, 2.5)
F1(D)	F_q	0.9764	0.9733	0.9718	0.9710	0.9708	0.9707	0.9706	0.9716	0.9738
	K_e	74.64	8.51	2.87	1.67	1.39	1.27	1.21	1.08	1.05
	K_e(see *a*)		9.78					1.22	1.09	1.05
	(k_f, k_r)	(9.47, 0.13)	(8.23, 0.97)	(6.68, 2.32)	(5.38, 3.22)	(4.77, 3.43)	(4.37, 3.43)	(4.10, 3.40)	(3.22, 2.98)	(2.66, 2.54)
F2(D)	F_q	0.9762	0.9731	0.9716	0.9709	0.9707	0.9706	0.9705	0.9715	0.9738
	K_e	75.06	8.53	2.88	1.67	1.39	1.27	1.21	1.08	1.05
	(k_f, k_r)	(9.47, 0.13)	(8.23, 0.97)	(6.68, 2.32)	(5.38, 3.22)	(4.77, 3.43)	(4.37, 3.43)	(4.10, 3.40)	(3.22, 2.98)	(2.66, 2.54)
F3(D)	F_q	0.9940	0.9920	0.9911	0.9906	0.9904	0.9904	0.9903	0.9905	0.9911
	K_e	4.65	2.14	1.46	1.20	1.13	1.09	1.07	1.03	1.02
	(k_f, k_r)	(7.90, 1.70)	(6.27, 2.93)	(5.34, 3.66)	(4.69, 3.91)	(4.34, 3.86)	(4.07, 3.73)	(3.88, 3.62)	(3.14, 3.06)	(2.62, 2.58)
F4(D)	F_q	0.9938	0.9918	0.9909	0.9905	0.9904	0.9903	0.9902	0.9905	0.9911
	K_e	4.67	2.15	1.46	1.20	1.13	1.09	1.07	1.03	1.02
	(k_f, k_r)	(7.91, 1.69)	(6.28, 2.92)	(5.34, 3.66)	(4.69, 3.91)	(4.34, 3.86)	(4.07, 3.73)	(3.88, 3.62)	(3.15, 3.05)	(2.62, 2.58)
F5(D)	F_q	0.9704	0.9653	0.9630	0.9618	0.9614	0.9612	0.9611	0.9623	0.9651
	K_e	348.81	18.30	4.19	2.00	1.57	1.39	1.29	1.11	1.06
	(k_f, k_r)	(9.57, 0.03)	(8.72, 0.48)	(7.27, 1.73)	(5.74, 2.86)	(5.01, 3.19)	(4.53, 3.27)	(4.22, 3.28)	(3.27, 2.93)	(2.68, 2.52)
F6(D)	F_q	0.9823	0.9811	0.9805	0.9803	0.9802	0.9801	0.9801	0.9808	0.9826
	K_e	16.06	3.97	1.97	1.39	1.24	1.17	1.13	1.05	1.03
	(k_f, k_r)	(9.04, 0.56)	(7.35, 1.85)	(5.97, 3.03)	(5.00, 3.60)	(4.53, 3.67)	(4.20, 3.60)	(3.97, 3.53)	(3.18, 3.02)	(2.64, 2.56)

Notes. [(a)] Lohr (1998); [(b)] Langer et al. (1984); [(c)] Smith & Adams (1980).

isotopologues are built automatically from the reactions involving the main isotope in the chemical code. The adopted method has first been presented in Le Bourlot et al. (1993), where statistical arguments were used to derive the various branching ratios in the chemical reactions. The procedure is limited to three carbon-containing molecules (oxygen-containing molecules have a maximum of two oxygen atoms in our chemical network) and does not disitinguish between C^{13}CC- or ^{13}CCC-containing species. A similar approach has recently been applied by Röllig & Ossenkopf (2013) for photon-dominated region models. However, Röllig & Ossenkopf (2013) used the old (LGFA84) exothermicity values. We also explicitly introduce the relation given by Langer et al. (1984) that $k_f + k_r = k_T$. The forward reaction k_f and reverse reaction k_r

Table 6. Isotopic fractionation ratios at 10 K for three H_2 densities, $n(H_2)$.

		Model A: LGFA84		Model B: Present results		
$n(H_2)$ (cm^{-3})	Species	$x^{a,b}$	R_A	$x^{a,b}$	R_B	δ (%)
10^4	$^{12}C^{16}O$	6.93(–5)		6.93(–5)		
	$^{13}C^{16}O$	1.15(–6)	60.1	1.15(–6)	60.1	
	$^{12}C^{18}O$	1.22(–7)	566	1.31(–7)	529	6.5
	$^{13}C^{18}O$	2.13(–9)	32 564	2.28(–9)	30 322	6.9
	$H^{12}C^{16}O^+$	7.74(–9)		7.72(–9)		
	$H^{13}C^{16}O^+$	1.54(–10)	50.3	1.74(–10)	44.2	12.0
	$H^{12}C^{18}O^+$	1.80(–11)	430	1.68(–11)	459	–6.7
	$H^{13}C^{18}O^+$	3.39(–13)	22 812	3.69(–13)	20 919	8.3
	$D^{12}C^{16}O^+$	2.08(–10)		2.06(–10)		
	$D^{13}C^{16}O^+$	3.60(–12)	57.7	5.13(–12)	40.2	30.4
	e^-	3.81(–8)		3.81(–8)		
10^5	$^{12}C^{16}O$	6.97(–5)		6.97(–5)		
	$^{13}C^{16}O$	1.16(–6)	60.1	1.16(–6)	60.2	
	$^{12}C^{18}O$	1.00(–7)	695	1.21(–7)	577	17.0
	$^{13}C^{18}O$	1.82(–9)	38 207	2.21(–9)	31 556	17.4
	$H^{12}C^{16}O^+$	3.01(–9)		2.98(–9)		
	$H^{13}C^{16}O^+$	7.70(–11)	39.1	1.05(–10)	28.5	27.1
	$H^{12}C^{18}O^+$	8.20(–12)	367	7.09(–12)	421	–14.7
	$H^{13}C^{18}O^+$	1.87(–13)	16 144	2.34(–13)	12 782	20.8
	$D^{12}C^{16}O^+$	7.45(–11)		7.29(–11)		
	$D^{13}C^{16}O^+$	1.30(–12)	57.2	2.93(–12)	24.8	56.6
	e^-	1.04(–8)		1.04(–8)		
10^6	$^{12}C^{16}O$	6.98(–5)		6.98(–5)		
	$^{13}C^{16}O$	1.16(–6)	60.0	1.16(–6)	60.1	
	$^{12}C^{18}O$	7.87(–8)	887	1.10(–7)	632	28.7
	$^{13}C^{18}O$	1.41(–9)	49 568	2.00(–9)	34 948	29.5
	$H^{12}C^{16}O^+$	1.02(–9)		9.97(–10)		
	$H^{13}C^{16}O^+$	3.33(–11)	30.6	5.67(–11)	17.6	42.5
	$H^{12}C^{18}O^+$	3.18(–12)	321	2.56(–12)	389	–21.1
	$H^{13}C^{18}O^+$	8.77(–14)	11 624	1.33(–13)	7480	35.7
	$D^{12}C^{16}O^+$	2.45(–11)		2.33(–11)		
	$D^{13}C^{16}O^+$	4.21(–13)	58.2	1.63(–12)	14.3	75.4
	e^-	3.03(–9)		3.03(–9)		

Notes. [a] Fractional abundances x are given relative to H_2. [b] Numbers in parentheses denote powers of 10.

rate coefficients involved in the isotopic exchange reaction are then evaluated from the total rate coefficient k_T as follows

$$k_f = k_T \frac{1}{1 + \exp(-\Delta E/k_B T)} \quad (27)$$

and

$$k_r = k_T \frac{\exp(-\Delta E/k_B T)}{1 + \exp(-\Delta E/k_B T)}. \quad (28)$$

These expressions have also been included in the study of fractionation in diffuse clouds presented by Liszt (2007).

The results summarized in Table 6 show that $CO/^{13}CO$ has the elemental value, whereas rarer isotopologues are very slightly depleted. The results for Models A and B are also very similar because no differences were used for the reaction rate coefficients between $^{13}C^+$ and CO. However, more significant are the differences for the results for the isotopic ratio of HCO^+, which directly arise from the variations of the exothermicities found in the present work. We also introduced a fractionation reaction for the deuterated isotope, whose rotational frequencies have been measured in the laboratory (Caselli & Dore 2005) and are detected in the interstellar medium (Guelin et al. 1982; Caselli et al. 2002). As the exothermicity of the deuterated isotopologues is somewhat higher, the isotopic ^{13}C ratio is somewhat lower than in the hydrogenic counterpart.

The general trend seen in Table 6 is that the new Model B predicts lower fractional abundances x for $H^{12}C^{16}O^+$ (up to 2%) and $D^{12}C^{16}O^+$ (up to 5%), lower relative abundances R_B of $H^{12}C^{18}O^+$ (7–21%), and higher relative abundances of the ^{13}C-containing isotopologues (up to 40% for the hydrogenic forms and up to 75% for the deuterated forms) than Model A.

4.3. Reaction of N_2 with N_2H^+

Molecular nitrogen is a homonuclear diatomic molecule with a $X^1\Sigma_g^+$ ground-electronic state with the three naturally occurring isotopologues: $^{14}N_2$, $^{14}N^{15}N$, and $^{15}N_2$. Whereas ^{14}N is a spin-1 boson, ^{15}N is a spin-1/2 fermion, such that the two symmetric

forms $^{14}N_2$ and $^{15}N_2$ follow different nuclear spin statistics. In the states with a higher nuclear spin degeneracy (ortho states), we have $g = (I_N + 1)(2I_N + 1)$, whereas $g = I_N(2I_N + 1)$ holds for the states with lower nuclear spin degeneracy (para states). To properly account for this effect, we evaluated the internal partition functions separately for even and odd J values,

$$Q_{\rm evenJ} = \sum_{J=0}^{\prime} \sum_i (2J+1)\, {\rm e}^{-\varepsilon_i^J/k_{\rm B}T}, \tag{29}$$

$$Q_{\rm oddJ} = \sum_{J=1}^{\prime} \sum_i (2J+1)\, {\rm e}^{-\varepsilon_i^J/k_{\rm B}T}, \tag{30}$$

where Σ' denotes summation in steps of 2. Multiplying each term by the appropriate nuclear spin (hyperfine) degeneracy factor, we obtain the partition function for N_2 as

$$Q_{\rm int}(^{14}N_2) = 6Q_{\rm evenJ} + 3Q_{\rm oddJ}, \tag{31}$$

$$Q_{\rm int}(^{15}N_2) = 3Q_{\rm oddJ} + Q_{\rm evenJ}. \tag{32}$$

$^{14}N^{15}N$ is not a homonuclear diatomic molecule, such that

$$Q_{\rm int}(^{14}N^{15}N) = 6\,(Q_{\rm evenJ} + Q_{\rm oddJ})\,. \tag{33}$$

The equilibrium constants K_e and rate coefficients for the isotopic variants of N_2H^+ reacting with N_2 are shown in Table 7. There we assumed the total rate coefficient k_T given by the Langevin collision rate (in SI units)

$$k_L = e\sqrt{\pi\,\alpha(N_2)/\mu_R\varepsilon_0}, \tag{34}$$

where e is the elementary charge, μ_R the reduced mass for the collision, and $\alpha(N_2)$ the polarizability of N_2 ($\alpha(N_2) = 1.710$ Å^3, Olney et al. 1997), giving thus $k_T = k_L = 8.11 \times 10^{-10}$ cm^3 s^{-1}. The rate coefficients k_f and k_r are determined from k_T and K_e with the help of Eqs. (24) and (25), respectively. Spectroscopic parameters of Trickl et al. (1995) and Bendtsen (2001) were used for the $X^1\Sigma_g^+$ states of $^{14}N_2$, $^{14}N^{15}N$, and $^{15}N_2$.

The nuclear spin degeneracy affects the equilibrium constants for the reactions involving either $^{14}N_2$ or $^{15}N_2$. At higher temperatures, K_e in Table 7 approaches 1/2 for reactions D2 and D3 having $^{14}N_2$ as a product, and 2 for reactions D4 and D5 having $^{15}N_2$ as a reactant. For reaction D1,

$$^{14}N_2H^+ + {}^{15}N_2 \underset{k_{-1}}{\overset{k_1}{\rightleftharpoons}} {}^{15}N_2H^+ + {}^{14}N_2, \tag{35}$$

the effects from nuclear spin statistics cancel out and $K_e^{(1)} \to 1$ as the temperature increases. From Eqs. (31) and (32), the ortho-to-para ratio is given by $R_{14} = 6Q_{\rm evenJ}/3Q_{\rm oddJ}$ for $^{14}N_2$ and by $R_{15} = 3Q_{\rm oddJ}/Q_{\rm evenJ}$ for $^{15}N_2$. We may note that R_{14} assumes a value of 2.41 (2.01) and R_{15} a value of 2.60 (2.99) at 5 K (10 K). At high temperature equilibrium, we have $R_{14} = 2$ and $R_{15} = 3$.

Adams & Smith (1981) employed normal nitrogen (ratio 2:1 of ortho vs. para $^{14}N_2$) in the SIFT experimental study of N_2H^++N_2. To measure the forward reaction and backward reaction rate coefficients at a given temperature, they interchanged the ion-source gas and reactant gas. Using mass-selected samples, these authors, however, were unable to distinguish between the isotopomers $^{14}N^{15}NH^+$ and $^{15}N^{14}NH^+$, such that their results provide the overall yield of these cations (no information on the relative yields). This applies to the competing reactions D2 and D3 on one side and the competing reactions D4 and D5 on the other side. $^{14}N^{15}NH^+$ and $^{15}N^{14}NH^+$ are expected to be differently fractionated (see Table 4).

To simulate the experimental conditions of Adams & Smith (1981), we introduced the overall forward k_{23} and overall reverse k_{-23} rate coefficients for reactions D2 and D3,

$$k_{23} = k_2 + k_3, \tag{36}$$

$$k_{-23} = \left[k_{-2}K_e^{(6)} + k_{-3}\right]\frac{1}{1+K_e^{(6)}}, \tag{37}$$

and the overall forward k_{45} and overall reverse k_{-45} rate coefficients for reactions D4 and D5,

$$k_{-45} = k_{-4} + k_{-5}, \tag{38}$$

$$k_{45} = \left[k_4K_e^{(6)} + k_5\right]\frac{1}{1+K_e^{(6)}}. \tag{39}$$

Here we explicitly assumed an equilibrium distribution between $^{14}N^{15}NH^+$ and $^{15}N^{14}NH^+$. The term $1 + K_e^{(6)}$ is the state-distribution normalization factor.

The variation of the rate coefficients with the temperature is displayed in Fig. 1. The common feature seen there is that the forward reaction becomes faster and the backward reaction slower with decreasing temperature. We also see that k_f and k_r exhibit a very weak temperature dependence for $T > 50$ K. For reactions D1 and D6, k_f and k_r approach the same value ($k_L/2$ in our model) at higher temperatures in Fig. 1a and Table 7. The high temperature limits of k_i and k_{-i} for $i = 2{-}5$ are, however, different because of the nuclear spin restrictions, as clearly seen in Figs. 1b,c. The reverse rate coefficients k_{-2} and k_{-3} in Fig. 1b become even higher than k_2 and k_3 for $T > 14.7$ K and $T > 3.4$ K, respectively, inverting thus the reaction direction. Herbst (2003) also found $k_{-3} > k_3$ at $T = 10$ K for reaction D3 assuming a different rate-coefficient model.

For the overall state-averaged rate coefficients in Fig. 1 and Table 7, we have $k_{23} > k_{-23}$ and $k_{45} > k_{-45}$ for all temperatures shown. This is in accordance with the SIFT experiment of Adams & Smith (1981). The rate coefficients $k_{\pm23}$ and $k_{\pm45}$ appear 30% higher than the experimental finding, reported with an error of ±25% at 80 K. Note, however, that the ratios k_{23}/k_{-23} and k_{45}/k_{-45} agree within 6% with the corresponding experimental values. Due to the nuclear spin angular momentum selection rules, the high-temperature limits (for $K_e^{(6)} \to 1$) of $k_{\pm23}$ and $k_{\pm45}$ are different from the high-temperature limits of $k_{\pm1}$ and $k_{\pm6}$.

From Eqs. (36)–(39) and the relationship of Eq. (11), we easily obtain

$$\frac{k_{23}}{k_{-23}} = K_e^{(2)} + K_e^{(3)} \tag{40}$$

and

$$\frac{k_{45}}{k_{-45}} = \frac{K_e^{(4)}K_e^{(5)}}{K_e^{(4)} + K_e^{(5)}}. \tag{41}$$

Following the procedure of Adams & Smith (1981), we may model the temperature dependence of the latter ratios as $e^{\Delta E_{ij}/k_BT}$ (compare with Eq. (5)). Using our results from Table 7 for the overall forward and overall reverse rate coefficients calculated at the temperatures of the SIFT experimental study, $T = 80$ K and $T = 292$ K, we derive $\Delta E_{23}, \Delta E_{45} = 6.5$ K for both reaction pairs.

Adams & Smith (1981) estimated the zero-point energy difference of 9 ± 3 K for reactions D2 and D4 (see Table 4). In accordance with the analysis presented here, we see, however, that the results of Adams & Smith (1981) should be attributed

Table 7. Equilibrium constants K_e, partition function factors F_q, and rate coefficients k_f, k_r (in 10^{-10} cm^3 s^{-1}) for the reactions of N_2H^+ with N_2.

Reaction	T (K)	5	10	20	40	60	80	100	200	292
D1	F_q	1.0561	0.9858	0.9834	0.9828	0.9826	0.9825	0.9825	0.9829	0.9840
	$K_e^{(1)}$	12.74	3.42	1.83	1.34	1.21	1.15	1.11	1.05	1.03
	(k_1, k_{-1})	(7.52, 0.59)	(6.28, 1.83)	(5.25, 2.86)	(4.65, 3.46)	(4.44, 3.67)	(4.33, 3.78)	(4.27, 3.84)	(4.15, 3.96)	(4.11, 4.00)
	$(k_f, k_r)^a$						(4.8, 4.1)			(4.1, 4.1)
D2	F_q	0.5101	0.4941	0.4934	0.4932	0.4931	0.4931	0.4931	0.4932	0.4937
	$K_e^{(2)}$	4.05	1.39	0.83	0.64	0.59	0.56	0.55	0.52	0.51
	(k_2, k_{-2})	(6.50, 1.61)	(4.72, 3.39)	(3.67, 4.44)	(3.16, 4.95)	(3.00, 5.11)	(2.92, 5.19)	(2.87, 5.24)	(2.77, 5.34)	(2.74, 5.36)
D3	F_q	0.5147	0.4989	0.4983	0.4982	0.4982	0.4982	0.4982	0.4982	0.4983
	$K_e^{(3)}$	0.78	0.55	0.52	0.52	0.51	0.51	0.51	0.50	0.50
	(k_3, k_{-3})	(3.54, 4.57)	(3.08, 5.03)	(2.89, 5.22)	(2.79, 5.32)	(2.76, 5.35)	(2.74, 5.37)	(2.73, 5.38)	(2.72, 5.39)	(2.71, 5.40)
	(k_{23}, k_{-23})	(10.05, 2.08)	(7.80, 3.89)	(6.56, 4.75)	(5.95, 5.12)	(5.76, 5.22)	(5.66, 5.28)	(5.60, 5.31)	(5.49, 5.37)	(5.45, 5.38)
	$(k_f, k_r)^a$						(4.6, 4.1)			(4.1, 4.1)
D4	F_q	2.0703	1.9952	1.9933	1.9929	1.9927	1.9927	1.9926	1.9928	1.9932
	$K_e^{(4)}$	3.15	2.46	2.21	2.10	2.06	2.05	2.03	2.01	2.01
	(k_4, k_{-4})	(6.16, 1.95)	(5.77, 2.34)	(5.59, 2.52)	(5.49, 2.62)	(5.46, 2.65)	(5.45, 2.66)	(5.44, 2.67)	(5.42, 2.69)	(5.41, 2.70)
D5	F_q	2.0521	1.9761	1.9734	1.9727	1.9724	1.9723	1.9722	1.9730	1.9748
	$K_e^{(5)}$	16.42	5.59	3.32	2.56	2.35	2.25	2.19	2.08	2.05
	(k_5, k_{-5})	(7.64, 0.47)	(6.88, 1.23)	(6.23, 1.88)	(5.83, 2.28)	(5.69, 2.42)	(5.61, 2.50)	(5.57, 2.54)	(5.48, 2.63)	(5.45, 2.66)
	(k_{45}, k_{-45})	(6.40, 2.42)	(6.11, 3.57)	(5.84, 4.40)	(5.65, 4.90)	(5.57, 5.07)	(5.53, 5.16)	(5.50, 5.22)	(5.45, 5.33)	(5.43, 5.36)
	$(k_f, k_r)^a$						(4.6, 4.1)			(4.1, 4.1)
D6	F_q	0.9912	0.9904	0.9901	0.9899	0.9898	0.9898	0.9898	0.9901	0.9908
	$K_e^{(6)}$	5.21	2.27	1.50	1.22	1.14	1.10	1.08	1.03	1.02
	(k_6, k_{-6})	(6.80, 1.31)	(5.63, 2.48)	(4.87, 3.24)	(4.45, 3.66)	(4.31, 3.80)	(4.24, 3.87)	(4.20, 3.91)	(4.12, 3.99)	(4.09, 4.02)

Notes. [a] Adams & Smith (1981).

to the reaction pairs {D2, D3} and {D4, D5}. This also explains a large discrepancy seen in Table 4 between the theoretical estimates and experimental finding for reaction D4.

In recent studies of Bizzocchi et al. (2010, 2013), $^{14}N^{15}NH^+$ and $^{15}N^{14}NH^+$ were both detected in a prototypical starless core L1544 of low central temperature and an abundance ratio $R_{15,14}^{14,15} = [^{14}N^{15}NH^+]/[^{15}N^{14}NH^+]$ of 1.1 ± 0.3 was derived. Note that the ratio $R_{15,14}^{14,15}$ correlates with $K_e^{(6)}$ describing reaction D6 of Eq. (12). As seen in Table 7, we obtain $K_e^{(6)}$ of 1.22–1.02 for T = 40–292 K; the additional calculation at T = 30 K gave $R_{15,14}^{14,15} = 1.31$. Also note that the earlier model of Rodgers & Charnley (2004) has led to the ratio $R_{15,14}^{14,15}$ of 1.8–2.3, which correlates with our $K_e^{(6)}$ value of 2.27 (1.72) at T = 10 K (15 K).

4.4. Ionic complexes

Ion-molecule reactions were additionally examined using electronic structure calculations, carried out for the linear approach of the neutral CO and N_2 to the linear cations HCO^+, HOC^+, and N_2H^+. The corresponding minimum-energy paths (MEPs) are displayed in Fig. 2. The MEPs are obtained optimizing three intramolecular distances for various monomer separations. Our calculations were performed at the CCSD(T)/aug-cc-pVTZ level of theory employing the standard MOLPRO and CFOUR optimization/threshold parameters.

The lower MEP in Fig. 2c is related to the reaction

$$N_2H^+ + CO \rightarrow HCO^+ + N_2, \quad (42)$$

which is considered to be the main destruction path for N_2H^+ when CO is present in the gas phase at standard abundances $[CO]/[H_2] \sim 10^{-4}$ (Snyder et al. 1977; Jørgensen et al. 2004). For this reaction, Herbst et al. (1975) reported a rate coefficient of 8.79×10^{-10} cm^3 s^{-1} at 297 ± 2 K. No reverse reaction was detected (Anicich 1993). For reactions involving HOC^+, Freeman et al. (1987) measured a rate coefficient k of 6.70×10^{-10} cm^3 s^{-1} for the following reaction

$$HOC^+ + CO \rightarrow HCO^+ + CO, \quad (43)$$

whereas Wagner-Redeker et al. (1985) reported k as 6.70×10^{-10} cm^3 s^{-1} for

$$HOC^+ + N_2 \rightarrow N_2H^+ + CO. \quad (44)$$

The Langevin collision rate is $k_L = 8.67 \times 10^{-10}$ cm^3 s^{-1} for reactions (42) and (43) involving CO and $k_L = 8.11 \times 10^{-10}$ cm^3 s^{-1} for reaction (44) involving N_2.

The common feature in Fig. 2 is the formation of a linear proton-bound ionic complex, which is 2000–7000 cm^{-1} more stable than the separated monomers. The properties of the complexes are summarized in Table 8, where we give the geometric parameters r_i, the equilibrium rotational constants B_e, the harmonic wavenumbers ω_i for the main and deuterated isotopologues, and the harmonic zero-point energies E_0. The corresponding results for the constituent monomers are listed in Table 9. Note that the monomer values E_0 in Table 9 are harmonic and therefore different from the anharmonic results of Table 1. The coordinates $r_i (i = 1–4)$ for A–B–H–C–D denote $r_1 = r(A-B)$, $r_2 = r(B-H)$, $r_3 = r(H-C)$ and $r_4 = r(C-D)$ in Table 8 and similar in Table 9. The dipole moments μ_z and the quadrupole moments Θ_{zz} in Table 8 and 9 are given with respect to the inertial reference frame with the origin in the complex centre of mass, where the position of the first

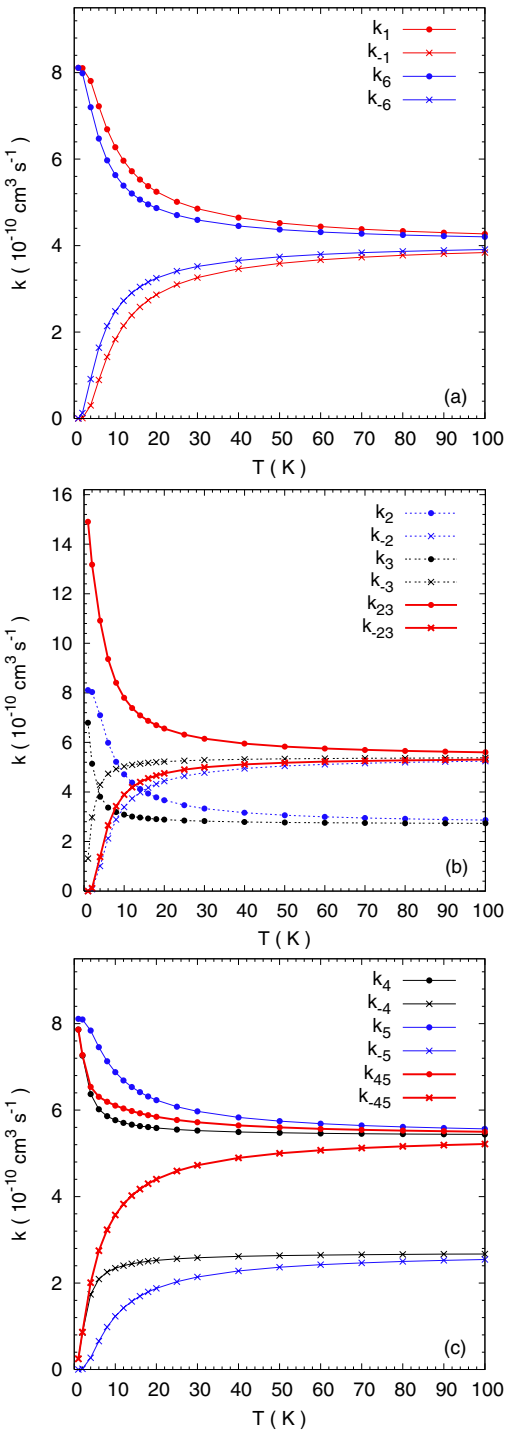

Fig. 1. Temperature dependence of the rate coefficients for $N_2H^+ + N_2$ for reactions D1 and D6 in **a)**, reactions D2 and D3 in **b)**, and reactions D4 and D5 in **c)**.

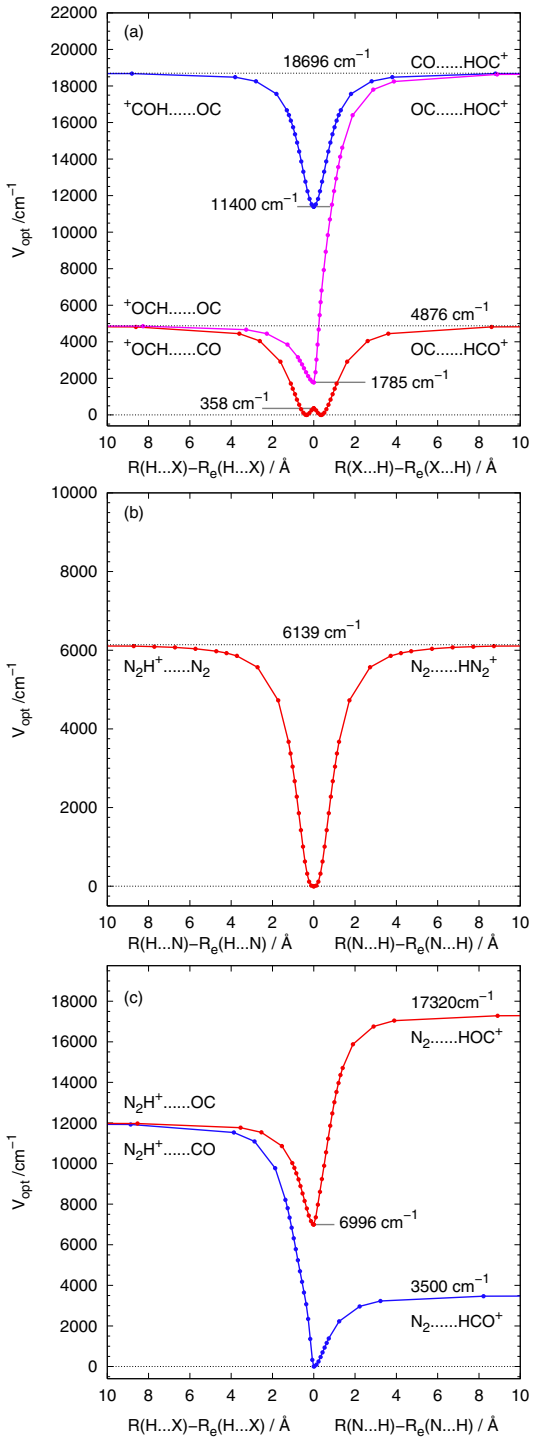

Fig. 2. Minimum energy paths for the linear approach of CO to HCO^+/HOC^+ in **a)**, for the linear approach of N_2 to HN_2^+ in **b)** and for the formation of the mixed linear cluster ions $N_2 \cdots HCO^+$ and $N_2H^+ \cdots OC$ in **c)**. The coordinate displayed on the x-axis is shown with the dotted line in the chemical formulas and X = O, C.

atom A of A–B–H–C–D or A–B–C along the z axis is chosen to be the most positive.

The ionic complexes $N_2HN_2^+$ and $COHOC^+$ have linear centrosymmetric equilibrium structures. The complex $OCH^+ \cdots CO$ is asymmetric with a barrier height to the centrosymmetric saddle point $OCHCO^+$(TS), seen at 358 cm^{-1} in Fig. 2a. In the mixed-cluster ions, the proton is bound either to CO, when $N_2 \cdots HCO^+$ is formed, or to N_2, when $N_2H^+ \cdots OC$ is formed. Comparison of Tables 8 and 9 shows that the geometric parameters experience prominent changes (up to 0.01–0.02 Å) upon complexation. In this fashion, the ionic (molecular) complexes differ from van der Waals complexes, in which the monomers preserve their geometric parameters to a great extent.

The transformations in Fig. 2 are all of the proton transfer type. The neutral CO may approach H^+ of the triatomic cation either with C or O since both C and O possess lone

Table 8. Properties of the ionic complexes from the CCSD(T)/aug-cc-pVTZ calculations.

Quantity	$OCH^+\cdots CO$	$OCHCO^+$(TS)	$OCH^+\cdots OC$	$COHOC^+$	$N_2\cdots HCO^+$	$N_2H^+\cdots OC$	$N_2HN_2^+$
r_1 (Å)	1.116	1.121	1.114	1.153	1.103	1.099	1.101
r_2 (Å)	1.175	1.387	1.118	1.194	1.774	1.104	1.276
r_3 (Å)	1.741	1.387	1.729	1.194	1.131	1.460	1.276
r_4 (Å)	1.125	1.121	1.146	1.153	1.114	1.149	1.101
B_e (cm^{-1})	0.0639	0.0681	0.0706	0.0948	0.0670	0.0844	0.0827
ω_1 (cm^{-1})	2464 (2397)	2306 (2305)	2887 (2520)	2081 (2081)	2745 (2480)	2555 (2466)	2402 (2402)
ω_2 (cm^{-1})	2237 (2237)	2273 (2272)	2136 (2076)	2015 (2014)	2351 (2351)	2079 (2059)	2365 (2365)
ω_3 (cm^{-1})	1730 (1291)	1290 (950)	2070 (1758)	1034 (745)	2077 (1658)	1945 (1474)	1235 (902)
ω_4 (cm^{-1})	1145 (859)	1290 (950)	984 (760)	1034 (745)	1040 (794)	1039 (767)	1235 (902)
ω_5 (cm^{-1})	1145 (859)	840i (600i)	984 (760)	988 (706)	1040 (794)	1039 (767)	438 (438)
ω_6 (cm^{-1})	271 (267)	395 (395)	193 (191)	467 (467)	229 (221)	271 (267)	265 (265)
ω_7 (cm^{-1})	271 (267)	295 (295)	189 (178)	134 (134)	229 (221)	214 (209)	265 (265)
ω_8 (cm^{-1})	199 (196)	295 (295)	189 (178)	134 (134)	195 (193)	214 (209)	159 (112)
ω_9 (cm^{-1})	131 (126)	148 (143)	91 (90)	89 (88)	117 (113)	103 (102)	144 (140)
ω_{10} (cm^{-1})	131 (126)	148 (143)	91 (90)	89 (88)	117 (113)	103 (102)	144 (140)
E_0 (cm^{-1})	4862 (4313)	4220 (3875)	4908 (4300)	4033 (3600)	5068 (4468)	4780 (4211)	4327 (3967)
μ_e (ea_0)	1.157	0	1.364	0	–1.389	0.808	0
Θ_{zz} (ea_0^2)	8.100	7.302	7.759	8.363	8.284	8.252	8.108

Notes. Wavenumbers for the deuterated species are given in parentheses.

Table 9. Properties of the monomers CO, N_2, HCO^+, HOC^+, and N_2H^+ from the CCSD(T)/aug-cc-pVTZ calculations.

Quantity	CO	HCO^+	HOC^+	N_2	N_2H^+
r_1 (Å)	1.136	1.094	0.992	1.104	1.099
r_2 (Å)		1.113	1.162		1.035
ω_1 (cm^{-1})	2144	3211 (2634)	3471 (2592)	2339	3395 (2711)
ω_2 (cm^{-1})		2192 (1923)	1931 (1861)		2276 (2052)
$\omega_{3,4}$ (cm^{-1})		844 (676)	61 (48)		686 (543)
E_0 (cm^{-1})	1072	3546 (2954)	2762 (2275)	1170	3522 (2924)
μ_e (ea_0)	–0.040	1.537	1.083	0	–1.328
Θ_{zz} (ea_0^2)	–1.466	4.235	4.198	–1.106	4.447

Notes. Wavenumbers for the deuterated species are given in parentheses. Vibrational modes (ω_3, ω_4) are doubly degenerate.

electron pairs. The proton attachment from the C side leads to a more stable complex. As seen in Fig. 2a, the complex $OCH^+\cdots OC$ is 1785 cm^{-1} above $OCH^+\cdots CO$ and 9615 cm^{-1} below $COHOC^+$. We also see that $N_2\cdots HCO^+$ is 6996 cm^{-1} more stable than $N_2H^+\cdots OC$. In all cases, the energy separation between the HCO^+- and HOC^+-containing complexes is smaller than the separation between free HCO^+ and HOC^+, seen to be 13 820 cm^{-1} in Fig. 2. The results of Fig. 2 are consistent with the fact that the proton tends to localize on the species with higher proton affinity. The experimental proton affinity is 594 kJ mol^{-1} (49 654 cm^{-1}) for CO on the C end and 427 kJ mol^{-1} (35 694 cm^{-1}) for CO on the O end (Freeman et al. 1987). The experimental proton affinity of 498 kJ mol^{-1} (41 629 cm^{-1}) was determined for N_2 (Ruscic & Berkowitz 1991).

The harmonic wavenumbers for the ionic complexes occurring in the course of reactions F1–F6 are provided in Table 10. In addition to the spectroscopic properties, we also give the harmonic zero-point energies of the complexes E_0, the reactants E_0^r, and the products E_0^p, as well as the dissociation energies including the harmonic zero-point energy correction in the direction of the reactants, $D_0^r = D_e + E_0^r - E_0$, and in the direction of the products, $D_0^p = D_e + E_0^p - E_0$, where D_e is the classical dissociation energy.

In Table 10, the vibrational mode ω_2, which is predominantly the diatom CO stretching vibration, is the most sensitive to isotopic substitutions. Compared with ω of free CO, ω_2 exhibits a blue-shift of 93 cm^{-1} for the main isotopologue (Table 9 vs. Table 8). The modes ω_1 and ω_3, highly sensitive to the H→D substitution (Table 8), can be considered as the H-C-O stretching modes. The intermolecular stretching mode is ω_8. The zero-point-corrected dissociation energies in Table 10 are approximately 240 cm^{-1} lower than the electronic dissociation energy of 4876 cm^{-1} (Fig. 2). The harmonic $\Delta E^h/k_B$ values in Table 10 and anharmonic $\Delta E/k_B$ values in Table 2 agree within 0.5 K.

The proton-bound complexes $OCH^+\cdots CO$ and $N_2\cdots HCO^+$ have large dipole moments μ_e of 1.16 ea_0 (2.94 D) and 1.39 ea_0 (3.53 D) (Table 8). For $OCH^+\cdots CO$, the most intense infrared transitions are expected for ω_3 (with harmonic intensity I_3^h of 2440 km mol^{-1}) and ω_1 (I_1^h = 536 km mol^{-1}), whereas the intermolecular stretch ω_8 has I_8^h = 232 km mol^{-1}. The fundamental (anharmonic) transitions ($\nu_1, \nu_2, \nu_3, \nu_{4,5}, \nu_{6,7}, \nu_8, \nu_{9,10}$) are calculated to be (2267, 2236, 1026, 1136, 346, 186, 208) for the main isotopologue (in cm^{-1}). The most intense infrared active transitions for $N_2\cdots HCO^+$ are ω_1 (I_1^h = 1034 km mol^{-1}), ω_3 (I_3^h = 814 km mol^{-1}), and ω_8 (I_8^h = 154 km mol^{-1}). For this complex, the fundamental vibrational ($\nu_1, \nu_2, \nu_3, \nu_{4,5}, \nu_{6,7}, \nu_8, \nu_{9,10}$)

Table 10. Isotopic variants of the ionic complex $OCH^+ \cdots CO$.

Quantity	16-12-H+13-16 reaction F1	18-12-H+13-18 reaction F2	16-12-H+12-18 reaction F3	16-13-H+13-18 reaction F4	16-12-H+13-18 reaction F5	18-12-H+13-16 reaction F6
ω_1 (cm^{-1})	2464	2426	2464	2409	2464	2426
ω_2 (cm^{-1})	2187	2133	2185	2133	2133	2187
ω_3 (cm^{-1})	1730	1712	1731	1728	1730	1712
$\omega_{4,5}$ (cm^{-1})	1145	1144	1147	1141	1149	1144
$\omega_{6,7}$ (cm^{-1})	267	264	271	261	266	265
ω_8 (cm^{-1})	198	191	197	193	194	195
$\omega_{9,10}$ (cm^{-1})	129	126	131	126	127	128
B_e (MHz)	1901	1728	1826	1799	1814	1812
E_0 (cm^{-1})	4830	4765	4836	4760	4798	4796
E_0^r (cm^{-1})	4594	4537	4592	4531	4568	4563
E_0^p (cm^{-1})	4581	4524	4587	4526	4550	4555
$\Delta E^h/k_B$ (K)	18.3	18.3	6.6	6.6	24.7	11.7
D_0^r (cm^{-1})	4640	4648	4632	4647	4645	4643
D_0^p (cm^{-1})	4627	4635	4627	4642	4628	4635

Notes. Here, *a*-*b*-H+*c*-*d* stands for ${}^aO^bCH^+ \cdots {}^cC^dO$. Vibrational modes (ω_4, ω_5), (ω_6, ω_7), and (ω_9, ω_{10}) are doubly degenerate.

transitions are determined to be (2357, 2321, 1876, 1045, 127, 186, 113) (in cm^{-1}). The anharmonic transitions are calculated from the cubic and semi-diagonal quartic force field in a normal coordinate representation by means of vibrational second-order perturbation theory, as implemented in CFOUR (Stanton et al. 2012).

Regarding the CCSD(T)/aug-cc-pVTZ method used here, we may note that our value of 358 cm^{-1} in Fig. 2a for the barrier height of OC+HCO^+ agrees reasonably well with previous theoretical results of 382 cm^{-1} (the CCSD(T)/cc-pVQZ approach of Botschwina et al. 2001) and 398 cm^{-1} (the CCSD(T)/aug-cc-pVXZ approach of Terrill & Nesbitt 2010 at the complete basis-set limit). A classical dissociation energy was previously determined to be 4634 cm^{-1} for $OCH^+ \cdots CO$ and 5828 cm^{-1} for $N_2HN_2^+$ at the complete basis-set limit (Terrill & Nesbitt 2010). The use of larger basis sets would ultimately be needed for converging theoretical results to stable values. Our primary goal here is the acquisition of first information relevant for the physical behaviour of the ionic complexes involving HCO^+ and N_2H^+. For these initial explorations of the PESs, the CCSD(T)/aug-cc-pVTZ approach is of satisfactory quality. A more detailed analysis of various basis-set effects, including the basis-set superposition error in systems with significantly deformed monomers, is being prepared and will be presented elsewhere.

5. Conclusion

Ion-molecule reactions are common in interstellar space, and investigating them helps to quantitatively understand the molecular universe (Watson 1976). We studied the isotope fractionation reactions of HCO^+/HOC^+ with CO and N_2H^+ with N_2, as well as the linear proton-bound complexes formed in the course of these reactions. For OCH^++CO, we pointed out inaccuracies of previous exothermicity values that are commonly employed in chemical networks. The new exothermicities affect particularly prominently the rate coefficients derived at temperatures of dark interstellar cloud environments, which markedly changes the abundance ratios of the ^{13}C- and ^{18}O-containing formyl isotopologues.

The linear proton-bound cluster ions are found to be strongly bound (2000–7000 cm^{-1}). The ionic complexes $OCH^+ \cdots CO$ and $OCH^+ \cdots N_2$ have sizeable dipole moments (2.9–3.5 D) and rotational constants of approximately 2000 MHz. If stabilized by means of collision and/or radiative processes, their high rotational population may facilitate the detection of these ions at low temperatures.

Acknowledgements. M.M. is grateful to Geerd H. F. Diercksen for sending her a copy of the MPI/PAE Astro 135 report. Marius Lewerenz is acknowledged for helpful discussions. Mila Lewerenz is thanked for helping with the literature search.

References

Adams, N. G., & Smith, D. 1981, ApJ, 247, L123
Anicich, V. G. 1993, J. Phys. Chem. Ref. Data, 22, 1469
Bendtsen, J. 2001, J. Ram. Spectrosc., 32, 989
Bizzocchi, L., Caselli, P., & Dore, L. 2010, A&A, 510, L5
Bizzocchi, L., Caselli, P., Leonardo, E., & Dore, L. 2013, A&A, 555, A109
Botschwina, P., Dutoi, T., Mladenović, M., et al. 2001, Faraday Discuss., 118, 433
Caselli, P., & Dore, L. 2005, A&A, 433, 1145
Caselli, P., Walmsley, C. M., Zucconi, A., et al. 2002, ApJ, 565, 331
Dalgarno, A., & Black, J. H. 1976, Rep. Prog. Phys., 39, 573
Freeman, C. G., Knight, J. S., Love, J. G., & McEwan, M. J. 1987, Int. J. Mass. Spectrum. Ion. Process., 80, 255
Guelin, M., Langer, W. D., & Wilson, R. W. 1982, A&A, 107, 107
Henning, P., Kraemer, W. P., & Diercksen, G. H. F. 1977, Internal Report, MPI/PAE Astro 135, Max-Planck Institut, München
Herbst, E. 2003, Space Sci. Rev., 106, 293
Herbst, E., Payzant, J. D., Schiff, H. I., & Bohme, D. K. 1975, ApJ, 201, 603
Huang, X., Valeev, E. F., & Lee, T. J. 2010, J. Chem. Phys., 133, 4108
Huber, K. P., & Herzberg, G. 1979, Molecular Spectra & Molecular Structure, Vol. IV. Constants of Diatomic Molecules (Englewood Cliffs, Prentice-Hall)
Hugo, E., Asvany, O., & Schlemmer, S. 2009, J. Chem. Phys., 130, 164302
Jørgensen, J. K., Schöier, F. L., & van Dishoeck, E. F. 2004, A&A, 416, 603
Langer, W. D., Graedel, T. E., Frerking, M. A., & Armentrout, P. B. 1984, ApJ, 277, 581
Le Bourlot, J., Pineau Des Forets, G., Roueff, E., & Flower, D. R. 1993, A&A, 267, 233
Liszt, H. S. 2007, A&A, 476, 291
Lohr, L. L. 1998, J. Chem. Phys., 108, 8012
Maret, S., Bergin, E. A., & Tafalla, M. 2013, A&A, 559, A53
Martin, J. M. L., Taylor, P. R., & Lee, T. J. 1993, J. Chem. Phys., 99, 286
Milam, S. N., Woolf, N. J., & Ziurys, L. M. 2009, ApJ, 690, 837

Mills, I., Cvitaš, T., Homann, K., Kallay, N., & Kuchitsu, K. 1993, Quantities, Units and Symbols in Physical Chemistry, 2nd edn. (Oxford: Blackwell Scientific Publications)
Mladenović, M., & Bačić, Z. 1990, J. Chem. Phys., 93, 3039
Mladenović, M., & Schmatz, S. 1998, J. Chem. Phys., 109, 4456
Olney, T. N., Cann, N. M., Cooper, G., & Brion, C. E. 1997, Chem. Phys., 223, 59
Pagani, L., Salez, M., & Wannier, P. G. 1992, A&A, 258, 479
Rodgers, S. D., & Charnley, S. B. 2004, MNRAS, 352, 600
Röllig, M., & Ossenkopf, V. 2013, A&A, 550, A56
Ruscic, B., & Berkowitz, J. 1991, J. Chem. Phys., 95, 4378
Schmatz, S., & Mladenović, M. 1997, Ber. Bunsenges. Phys. Chemie, 101, 372
Smith, D., & Adams, N. G. 1980, ApJ, 242, 424
Snyder, L. E., Hollis, J. M., & Watson, W. D. 1977, ApJ, 212, 79
Špirko, V., Bludský, O., & Kraemer, W. P. 2008, Collect. Czech. Chem. Commun., 73, 873
Stanton, J. F., Gauss, J., Harding, M. E., et al. CFOUR, a quantum chemical program package, http://www.cfour.de
Terrill, K., & Nesbitt, D. J. 2010, Phys. Chem. Chem. Phys., 12, 8311
Terzieva, R., & Herbst, E. 2000, MNRAS, 317, 563
Trickl, T., Proch, D., & Kompa, K. L. 1995, J. Mol. Spectrosc., 171, 374
Urey, H. C. 1947, J. Chem. Soc., 562
Wagner-Redeker, W., Kemper, P. R., Jarrold, M. F., & Bowers, M. T. 1985, J. Chem. Phys., 83, 1121
Watson, W. D. 1976, Rev. Mod. Phys., 48, 513
Werner, H.-J., Knowles, P. J., Knizia, G., et al. 2012, MOLPRO, a package of ab initio programs, http://www.molpro.net